Structure of Aqueous Mixtures of *N*,*N*-Dimethylacetamide Studied by Infrared Spectroscopy, X-ray Diffraction, and Mass Spectrometry

Toshiyuki Takamuku,*,† Daisuke Matsuo,† Masaaki Tabata,† Toshio Yamaguchi,‡ and Nobuyuki Nishi§

Department of Chemistry, Faculty of Science and Engineering, Saga University, Honjo-machi, Saga 840-8502, Japan, Advanced Materials Institute and Department of Chemistry, Faculty of Science, Fukuoka University, Nanakuma, Jonan-ku, Fukuoka 814-0180, Japan, and Institute for Molecular Science, Myodaiji, Okazaki 444-8585, Japan

Received: December 31, 2002; In Final Form: April 6, 2003

Infrared (IR) spectroscopy and X-ray diffraction measurements have been performed at 298 K on mixtures of *N*,*N*-dimethylacetamide (DMA) and water over the entire range of DMA mole fractions (x_{DMA}). Mass spectra have also been measured on the clusters that have been isolated by the adiabatic expansion of liquid droplets of the mixtures. The IR overtone band of the C═O stretching vibration for the DMA−D_2O mixtures and the O−D stretching band of HDO for the DMA−H_2O mixtures containing 5% D_2O both shifted to lower frequencies as the water content increased, accompanied by two inflection points, at $x_{DMA} = 0.1$ and 0.6. These results suggested that hydrogen bonding between the C═O group and the water molecules and structural changes of predominant solvent clusters were taking place at these specific mole fractions. The X-ray radial distribution functions have indicated that the structure of the predominant solvent clusters in the mixtures could be classified into four regimes: (1) $0 < x_{DMA} \leq 0.1$, where the water clusters predominate; (2) $0.1 < x_{DMA} \leq 0.3$, where more water clusters than DMA clusters are formed; (3) $0.3 < x_{DMA} \leq 0.6$, where the DMA structure becomes predominant but the water clusters still remain; and (4) $0.6 \leq x_{DMA} \leq 1$, where the DMA clusters are dominant in the mixtures. On the basis of the present results on the microscopic structure of the mixtures, the anomalies of thermodynamic parameters such as the enthalpy of mixing are discussed.

Introduction

Aqueous *N*,*N*-dimethylacetamide (DMA) mixtures have often been used as solvents in various chemical reactions, and its physicochemical parameters, such as ^{1}H NMR chemical shift, density, viscosity, dielectric permittivity, molar volume, and surface tension, have been compiled.[1] One of the interesting behaviors of the mixtures is that anomalies occur at 33 mol % in all the aforementioned parameters. The anomalies have been interpreted by the formation of a hydrogen-bonded complex, DMA·$2H_2O$, the composition of which corresponds to a DMA mole fraction (x_{DMA}) of 0.33.[1] Recent calorimetric measurements of 15-crown-5[2] and benzo-15-crown[3] in aqueous DMA mixtures have shown that the enthalpy of solution exhibits a maximum at $x_{DMA} \approx 0.4$; i.e., the enthalpy gradually increases as x_{DMA} decreases in the range of $0.4 < x_{DMA} \leq 1$ but drastically decreases below $x_{DMA} \approx 0.4$. The hydrophobic hydration of the solutes was proposed to explain the behavior of the solution enthalpies. However, no detailed structural evidence has been shown at the molecular level.

So far, we have applied X-ray diffraction (XRD), mass spectrometry, and small-angle neutron scattering to various aqueous mixtures of organic solvents, such as methanol,[4] ethanol,[5−7] 1,4-dioxane,[8] and acetonitrile,[9−11] and clarified the microscopic structure of the predominant clusters in the mixtures, by which the anomalies of thermodynamic parameters have been successfully discussed.

In the present study, the structure of aqueous mixtures of DMA has been investigated; the DMA molecule has one oxygen atom as a hydrogen-bonding acceptor, but not a hydrogen-bonding donor, as well as a 1,4-dioxane molecule and a large dipole moment (12.4×10^{-30} Cm) that is similar to that for acetonitrile (13.06×10^{-30} Cm). Three methods have been performed on DMA−water mixtures to clarify how the two characteristics of the DMA molecule affect the mixing state at the molecular level. Fourier transform infrared (FT-IR) spectroscopy has been used to investigate the hydrogen bonding between DMA and water in DMA−water mixtures as a function of x_{DMA}, and XRD measurements have been made on the DMA−water mixtures to derive direct structural information, in terms of the interatomic distance and the coordination number of the predominant clusters in the mixtures. To obtain information on molecular compositions of predominant clusters formed in the mixtures, mass spectra have been measured on the clusters isolated in the vacuum by the adiabatic expansion of liquid droplets composed of DMA and water molecules. On the basis of all results obtained in this study, possible structural changes of predominant clusters in the DMA−water mixtures are discussed at the molecular level. The anomaly of the enthalpies of mixing for DMA−water mixtures at 298 K is also discussed on the basis of the structural change of the mixtures.

Experimental Section

Sample Solutions. DMA (extra grade, Tokyo Kasei Industry) was dried with thermally activated 4 Å molecular sieves for

* Author to whom correspondence should be addressed. E-mail: takamut@cc.saga-u.ac.jp.
† Saga University.
‡ Fukuoka University.
§ Institute for Molecular Science.

10.1021/jp0226578 CCC: $25.00
Published on Web 05/31/2003

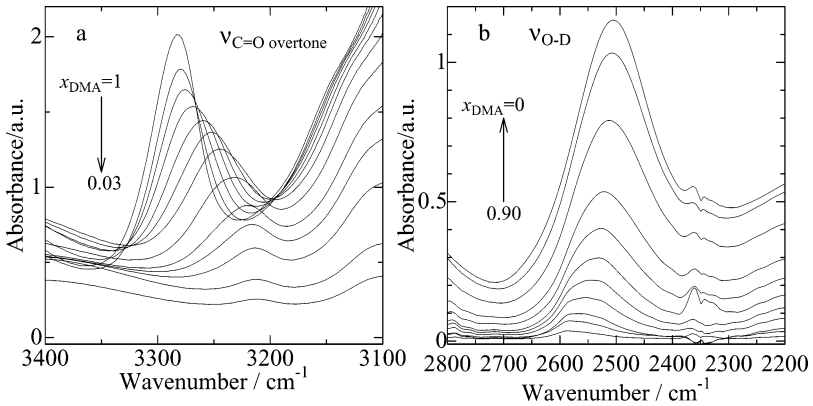

Figure 1. IR absorption spectra of (a) DMA in the DMA−D_2O mixtures at x_{DMA} = 0.03, 0.05, 0.10, 0.15, 0.20, 0.30, 0.40, 0.50, 0.60, 0.70, 0.80, 0.90, and 1, and (b) HDO in the mixtures of DMA with water containing 5% D_2O at x_{DMA} = 0, 0.05, 0.10, 0.20, 0.30, 0.40, 0.50, 0.60, 0.70, 0.80, and 0.90.

several days and then distilled at 313 K under reduced pressure. D_2O (deuterium atom content of 99.9%, CEA) was used without further purification. The water was distilled twice. Samples of the DMA−water mixtures were prepared by weighing DMA, water, and/or D_2O to the required x_{DMA} values.

IR Measurements. The overtone spectrum of the C═O stretching band of DMA was recorded at 298 K for pure DMA and DMA−D_2O mixtures at x_{DMA} = 0.03, 0.05, 0.10, 0.15, 0.20, 0.30, 0.40, 0.50, 0.60, 0.70, 0.80, and 0.90 with an FT-IR spectrophotometer (Perkin−Elmer model SPECTRUM 2000). The O−D stretching band of HDO was also measured on mixtures of DMA with H_2O containing 5% D_2O at x_{DMA} = 0, 0.05, 0.10, 0.20, 0.30, 0.40, 0.50, 0.60, 0.70, 0.80, and 0.90. The sample solution was kept in a cell with CaF_2 windows, and the sample thickness was adjusted with Teflon spacers (0.5 and 0.025 mm) for the measurements of C═O and O−D bands, respectively. The errors in wavenumber were estimated to be less than ±0.5 cm^{-1}.

X-ray Diffraction Measurements. XRD measurements were performed at 298 K on pure DMA and DMA−water mixtures at x_{DMA} = 0.03, 0.05, 0.077, 0.10, 0.15, 0.20, 0.25, 0.30, 0.40, 0.50, 0.60, 0.70, 0.80, and 0.90 on a rapid liquid X-ray diffractometer with an imaging plate (IP) as a two-dimensional detector (BRUKER AXS model DIP301). Densities for the sample solutions were measured at 298 K using a densitometer (ANTON Paar K. G., DMA60). Details of the X-ray diffractometer have been described elsewhere.[12,13] X-rays were generated at a rotary molybdenum anode (Rigaku model RU-300) that was operated at 50 kV and 200 mA and then monochromatized by a flat graphite crystal to obtain MoKα radiation (at a wavelength, λ, of 0.7107 Å). X-ray scattering intensities for a sample solution sealed in a glass capillary with an inner diameter of 2 mm (wall thickness of 0.01 mm) were accumulated on the IP for 1 h. The observed range of the scattering angle (2θ) was 0.2°−109°, corresponding to the scattering vector s (which is equal to $4\pi\lambda^{-1}\sin\theta$) of 0.03−14.4 Å^{-1}. X-ray intensities for an empty capillary were also measured as background.

Two-dimensional X-ray data ($I_{obsd}(x,y)$, where x and y are horizontal and vertical coordinates, measured on the IP) were integrated into one-dimensional data ($I_{obsd}(\theta)$) after correction for polarization, as previously reported.[12] The observed intensities for the samples and empty capillary were also corrected for absorption.[13] The contribution of the sample solution alone was obtained by subtracting the intensities for the empty capillary from those for the sample. The corrected intensities were normalized to absolute units by conventional methods.[14−16] The structure function, $i(s)$, was calculated using eq 1 in ref 9. In the data treatment, the stoichiometric volume V was chosen to contain one oxygen atom from both DMA and water in the systems. The structure function was Fourier-transformed to the radial distribution function $D(r)$ in a usual manner.[9] To perform a quantitative analysis of the X-ray data, a comparison between the experimental structure function and the theoretical one, which was calculated on a structure model using eq 5 in ref 9, was made by a least-squares refinement procedure, using eq 4 in ref 9. The present XRD data were treated using the programs KURVLR[17] and NLPLSQ.[18]

Mass Spectrometry. Mass spectrometric measurements were performed on DMA−water mixtures at x_{DMA} = 0.005, 0.01, 0.02, 0.03, 0.05, 0.077, 0.10, 0.20, 0.40, and 0.60. Details of the mass spectrometer have been previously described.[19−22] A flow of liquid droplets was generated by the hydrodynamic conversion of liquid from a notched small nozzle with a diameter of ~40 μm. These droplets were introduced into vacuum chambers through two skimmers and adiabatically expanded in the ionization chamber to produce isolated clusters, followed by electron impact ionization at 40 eV. The droplet beam was introduced perpendicular to the repeller electrode, which was operated at 3400 V. A double focus spectrometer with electric and magnetic sectors (Kratos Analytical, Profile) was used to measure the intensity distribution of the isolated clusters in a mass-number range of $100 \le m/Z \le 900$.

The average temperature of the liquid droplets was estimated by the mass spectral change of an aqueous solution of propionic acid with an acid mole fraction of 0.005, as have previously been described.[21,22] In the present measurements, the temperature of liquid droplets was set at 308 K, and the lower limit of the average droplet temperature was found to be 303 K.

One should remember that the clusters observed in the mass spectra suffer from dissociation by electron impact and might not have the same features as clusters formed in the corresponding bulk solutions. However, in our previous investigations, the mass spectra for aqueous mixtures of methanol,[4] ethanol,[5−7] and 1,4-dioxane[8] have shown that the short-range ordering feature of the clusters obtained from the mass spectrometry agrees well with that obtained from XRD experiments on the corresponding bulk mixtures.

Results and Discussion

IR Spectra. Figure 1a shows the IR absorption spectra for pure DMA and DMA−D_2O mixtures of various x_{DMA} values. For pure DMA, a sharp band at 3283 cm^{-1} is assigned to the

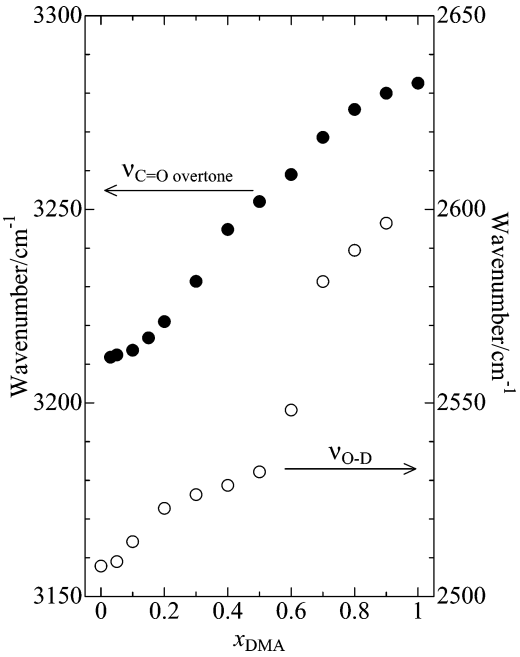

Figure 2. Wavenumbers of the overtone $\nu_{C=O}$ mode of the DMA molecules and the ν_{O-D} mode of the HDO molecules as a function of x_{DMA}. The estimated errors in the wavenumbers are less than ± 0.5 cm^{-1}.

overtone frequency of the C═O stretching vibration ($\nu_{C=O}$) of a DMA molecule.[23,24] A large wing observed below ~3200 cm^{-1} is due to the C−H stretching band of the methyl group.[24] The intensity of the wing is gradually weakened as the DMA concentration decreases. The overtone $\nu_{C=O}$ band also decreases and shifts to lower wavenumbers as the D_2O concentration increases. This shift suggests the formation of hydrogen bonds between the C═O group and water molecules, because the C═O bond would be slightly weakened by the hydrogen bonding. Enhancement of the hydrophobic DMA−DMA interaction also can be considered to contribute to the lower-wavenumber shift of the $\nu_{C=O}$ band, because DMA−DMA interaction is promoted at the high values of x_{DMA}, as will be discussed in the section on mass spectrometry that is presented later in this paper.

Figure 1b shows the O−D absorption band of HDO in the aqueous DMA mixtures containing 5% D_2O. In the spectrum of pure water ($x_{DMA} = 0$), a strong band at 2508 cm^{-1} arises from the O−D stretching mode (ν_{O-D}) of HDO.[9] On the other hand, in the spectrum for the DMA−water mixture at $x_{DMA} = 0.90$, the ν_{O-D} band is substantially weakened and shifted to 2596 cm^{-1}. This band at 2508 cm^{-1} is ascribed to the ν_{O-D} of HDO molecules hydrogen-bonded with other water molecules or a C═O group of a DMA molecule, as described below. It has been reported that the ν_{O-D} band of monomeric HDO molecules appears at a higher wavenumber (2680 cm^{-1}) in benzene.[25]

Figure 2 shows plots of the wavenumbers of the aforementioned two bands (overtones $\nu_{C=O}$ and ν_{O-D}) as a function of x_{DMA}. The wavenumber of the $\nu_{C=O}$ mode gradually decreases from 3283 cm^{-1} to 3214 cm^{-1} when the value of x_{DMA} is changed from 1 to 0.10; however, the wavenumber becomes almost constant at $x_{DMA} \leq 0.10$. This change suggests that DMA−DMA interaction is gradually enhanced by the hydrophobic effect at $x_{DMA} = 0.90-0.10$ and that DMA molecules that are hydrogen-bonded with water molecules also increase in the lower x_{DMA} range. At $x_{DMA} \leq 0.10$, in particular, the change in the wavenumber of the $\nu_{C=O}$ mode reveals that the hydrogen bonds between DMA and water molecules are almost saturated.

The tendency of the ν_{O-D} wavenumber to decrease with decreasing x_{DMA}, from 0.90 to 0.70, is similar to that for the $\nu_{C=O}$ band in the same x_{DMA} range. This observation indicates hydrogen bonding of water molecules to the carbonyl oxygen atoms of DMA molecules. In addition, hydrogen bonds among the water molecules are formed in the mixtures. However, a sudden decrease in the ν_{O-D} wavenumber is seen at $x_{DMA} = 0.60$. This suggests that the tetrahedral-like structure of water begins to form in the mixtures at $x_{DMA} = 0.60$, because a sufficient amount of water molecules is available. In the range of $0.20 \leq x_{DMA} \leq 0.50$, the wavenumbers of both modes moderately decrease as the water concentration increases, suggesting an increase in the number of both types of hydrogen bonds. Another sudden change in the wavenumber of the ν_{O-D} mode is seen at $x_{DMA} = 0.10$. This observation reveals that the tetrahedral-like structure of water becomes dominant at $x_{DMA} \leq 0.10$, as discussed for the $\nu_{C=O}$ overtone band.

X-ray Diffraction. The *s*-weighted structure functions $i(s)$ of pure DMA and the DMA−water mixtures at various x_{DMA}, together with that of water[4] for comparison, are depicted in Figure S1 in the Supporting Information. Figure 3 shows the corresponding radial distribution functions (RDFs) in the $D(r) - 4\pi r^2\rho_0$ form (solid lines). In the RDF for DMA ($x_{DMA} = 1$), two dominant peaks are observed, at 1.4 and 2.4 Å, which are assigned to intramolecular C^1═O, C^1−N, C^3(C^4)−N, and C^1−C^2 bonds and nonbonding N···O, C^1···C^3(C^4), C^2···O, C^3···C,[4] and C^2···N interactions within a DMA molecule, respectively. The notation of carbon atoms is shown in Figure 4. All intramolecular distances in a DMA molecule were taken from a gas electron diffraction and computer simulation study of DMA[26] and are summarized in Table S1 in the Supporting Information. The molecular conformation of DMA seen in the gas phase will be retained in the liquid phase, as has been found for related *N*,*N*-dimethylformamide (DMF),[27] because the C−N bond within both DMA and DMF is conjugated with the C═O bond and, hence, has, in part, double bond nature to prevent free rotation of the C−N bond. A very broad and weak hump observed over the *r*-range of 3.8−8 Å arises mainly from intermolecular interactions among DMA molecules in the liquid.

In Figure 3, the contribution of all the intramolecular interactions of the DMA and water[28] molecules (Table S1, Supporting Information) was subtracted from the original RDFs (solid lines) for the mixtures, to extract the intermolecular RDFs (IRDFs, dashed lines). In the IRDFs, when water is added to DMA, a hump at 2.8 Å gradually evolves, in particular, growing as a peak at $x_{DMA} \approx 0.60$. This peak has often been observed as the first-neighbor O···O interactions in pure water[29,30] and aqueous solutions.[4−9,11] In the previous section, the IR data have also suggested the formation of hydrogen bonds between the DMA and water molecules. To our knowledge, there are no data on the O···O distances between DMA and water molecules. However, because of the larger Gutmann donor number of DMA (27.8), relative to that of water (18.0),[31] and the large Mayer−Gutmann acceptor number of water (54.8),[31] the O···O bond length between the DMA and water molecules should not be very different from that for the water−water hydrogen bonds (2.83 Å).[4] Thus, the 2.8 Å peak seen in the IRDFs should be ascribed to the O···O hydrogen bonds of both water−water and DMA−water.

At $x_{DMA} = 0.40$ and 0.50, the broad and weak hump at 3.8−8 Å, which is characteristic of DMA, still remains but becomes weaker. At $x_{DMA} \leq 0.30$, the peak at 2.8 Å significantly grows, and a valley appears at 5.7 Å in the middle of the broad hump

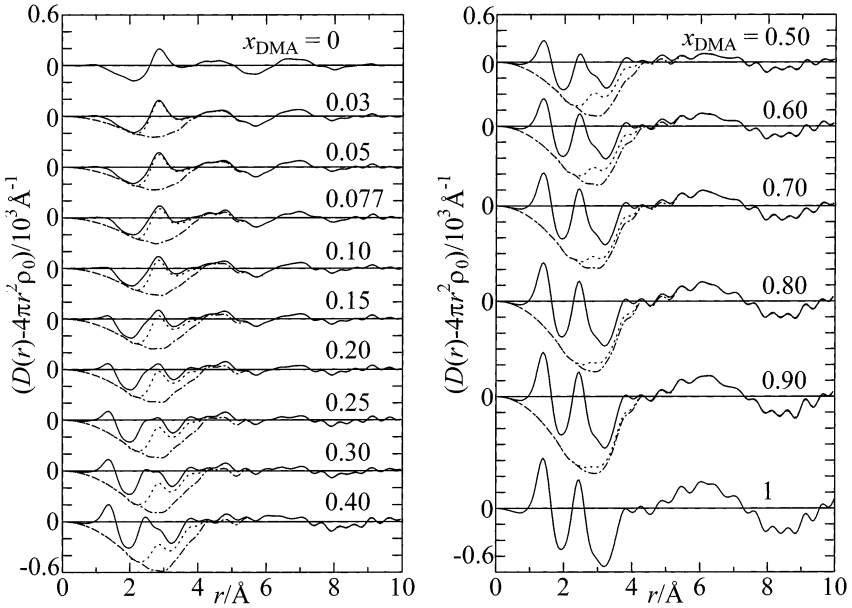

Figure 3. Radial distribution functions in the $D(r) - 4\pi r^2\rho_0$ form for DMA, water, and their mixtures at various x_{DMA}. Solid lines represent experimental values (original RDFs), dashed lines are intermolecular RDFs (IRDFs) obtained by subtraction of intramolecular interactions within the DMA and water molecules from the original RDFs, and dotted−dashed lines are residual curves after subtraction of theoretical values calculated using optimized parameter values (Table S2, Supporting Information) from the IRDFs.

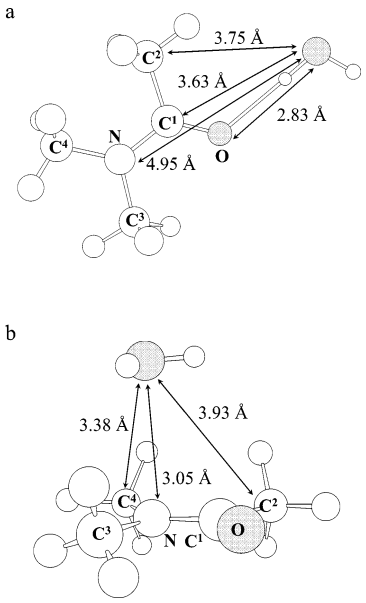

Figure 4. Structure models of (a) the hydrogen bond and (b) the dipole−dipole interaction between the DMA and water molecules, with important distances noted.

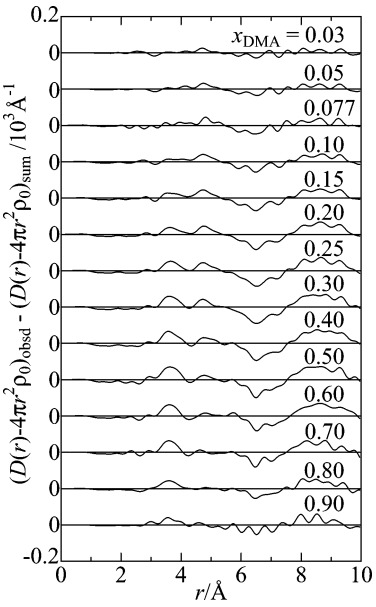

Figure 5. Residual RDFs obtained from subtracting a weighted sum of RDFs for pure DMA and pure water from the original RDFs.

at 3.8−8 Å, resulting in a hump at 7 Å that is assigned to the third neighbor of the hydrogen bonds among water molecules. In particular, at $x_{DMA} \leq 0.10$, the RDFs become similar to that for pure water ($x_{DMA} = 0$), suggesting that the tetrahedral-like structure of water becomes dominant in the mixtures.

It is difficult to determine a unique structure of DMA and the DMA−water mixtures from the present RDFs and IRDFs, because no significant ordering of DMA molecules might be present. Thus, the first attempt made was to determine if the RDFs of the DMA−water mixtures can be reproduced as a weighted sum of those of pure DMA and pure water, given by eq 1:

$$[D(r) - 4\pi r^2\rho_0]_{sum} = f_{DMA}[D(r) - 4\pi r^2\rho_{0,DMA}]_{DMA} + f_{Water}[D(r) - 4\pi r^2\rho_{0,Water}]_{Water} \quad (1)$$

where f_{DMA} (equal to $\rho_{0,Mix}/\rho_{0,DMA}$) and f_{Water} (equal to $\rho_{0,Mix}/\rho_{0,Water}$) are the weights for correction of the differences in the average electron densities among the binary mixtures, DMA, and water; $\rho_{0,Mix}$, $\rho_{0,DMA}$, and $\rho_{0,Water}$ represent the average electron densities in the stoichiometric volume for the mixtures, DMA, and water, respectively. Figure 5 shows the residual RDFs (which are equal to the original RDF minus the sum). As seen in Figure 5, the residual RDFs in the range of $x_{DMA} > 0.10$ show a broad positive peak at 3.6 Å and a negative peak at 7 Å. In addition, another positive peak appears at 4.9 Å in the residual RDFs in the range of $x_{DMA} < 0.50$. These features in the residual RDFs clearly suggest that the structure of the DMA−water mixtures is not described as the weighted sum of those of pure DMA and pure water.

The positive peaks at 3.6 and 4.9 Å show new interactions in the DMA−water mixtures. As discussed in the IR data

section, the new interactions should arise from the interatomic interactions between the DMA and water molecules. Figure 4a depicts one of the possible models of hydrogen bonding between the DMA and water molecules; the location of H_2O at a distance of 2.83 Å for the O(C═O)···O(H_2O) hydrogen bond gives rise to distances of 3.63, 3.75, and 4.95 Å for the nonbonding C^1···O, C^2···O, and N···O interactions, respectively. Apparently, however, this model alone is not sufficient to explain the positive peak at 3.6 Å. Thus, another contributor should be considered. The dipole moments of the DMA and water molecules are 12.4×10^{-30} and 6.47×10^{-30} Cm, respectively; therefore, it is very likely that the dipole−dipole interaction is also responsible for the DMA−water interaction. Figure 4b shows an antiparallel dipole−dipole arrangement, in which a water molecule is situated over the nitrogen atom of a DMA molecule at a distance of 3.05 Å, as estimated from the van der Waals radii of 1.4, 1.5, and ∼2.0 Å for oxygen, nitrogen, and CH_3, respectively, within a DMA molecule and that of a water molecule (∼1.5 Å). In this model, the C^1···O, C^2···O, C^3···O, C^4···O, and O···O interactions between the DMA and water molecules are estimated to be 3.34, 3.93, 3.38, 3.38, and 3.80 Å, respectively. The negative peaks from 6 to 7.5 Å in Figure 5 may be caused by a decrease of the third-neighbor O···O interactions in the tetrahedral-like structure of water, because the water concentration in the mixtures is less than that in bulk water. At $x_{DMA} \leq 0.10$, the negative peaks become less pronounced, because the bulk water structure predominates in the DMA−water mixtures.

To perform a quantitative analysis on the O···O hydrogen bonds of DMA−water and water−water formed in the DMA−water mixtures, a model-fitting procedure was applied to the structure functions for the mixtures in Figure S1 (in the Supporting Information). In the liquid state, various conformations for DMA−water interactions would be possible; thus, the previously mentioned two conformations should not be regarded as limited ones. It is difficult to construct a unique model for a conformation between DMA and water molecules. Therefore, first, to search for the most likely structure models, two different types of DMA−water interactions (hydrogen bond (Figure 4a) and dipole−dipole (Figure 4b)), and bulk water characterized by the tetrahedral-like arrangement with the interstitial interactions,[4] were modified to fit the IRDFs well in the range of $r \leq 5$ Å. Consequently, the most likely structure models could be obtained only by modifying the numbers of the O···O hydrogen bonds of DMA−water and water−water, the other interatomic interactions between DMA and water molecules, and the interstitial water molecules; however, the distances and temperature factors were fixed as follows. The distance of the O···O hydrogen bonds was fixed to 2.83 Å with a temperature factor of 0.017 $Å^2$, whereas those of the C^1···O, C^2···O, C^3···O, C^4···O, N···O, and O···O interactions between DMA and water molecules were fixed to the values given in Figure 4, with a temperature factor of 0.030 $Å^2$. The parameters for the interstitial water molecule were set to a distance of 3.35 Å and a temperature factor of 0.015 $Å^2$, as previously estimated from XRD measurements on pure water.[4] Next, least-squares refinement calculations were made on the structure functions over the *s*-range from 4.0 to 14.4 $Å^{-1}$, using the model parameters primarily obtained. The distance and coordination number for the O···O hydrogen bonds were varied independently. For the data at $x_{DMA} \geq 0.40$, the O···O distance could not be optimized, because of its small contribution to the peak. Thus, the distance was fixed to 2.83 Å.

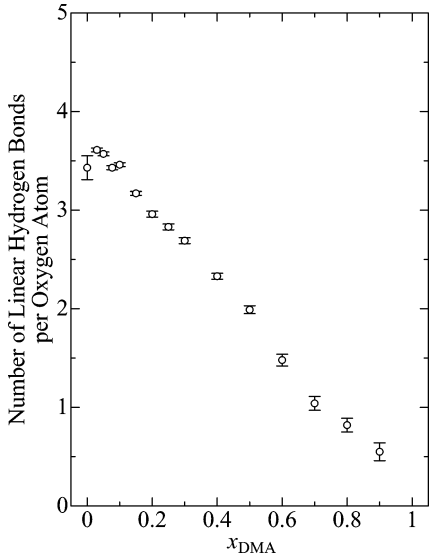

Figure 6. Dependence of x_{DMA} on the coordination number per oxygen atom within both DMA and water molecules. The standard deviations (σ) were indicated as error bars.

The final optimized parameter values are listed in Table S2 in the Supporting Information. Figure S1 in the Supporting Information shows a satisfactory agreement between the model and the experimental values, except for the range of $s \leq 3.5$ $Å^{-1}$, in which the long-range interactions were not taken into account in the present analysis. In Figure 3, the subtraction of the theoretical peaks from the IRDFs has given smooth residual curves over the *r*-range from 0 to 4.0 Å, indicating that no other significant interactions are present in the *r*-range of interest.

Recall that the parameter values for the O···O hydrogen bonds listed in Table S2 (in the Supporting Information) are average values for those of DMA−water and water−water interactions. The average O···O distance (2.83 Å) does not significantly change over the entire range of x_{DMA}. On the other hand, the coordination number of the O···O bonds increases as the value of x_{DMA} decreases or the water content increases.

In Figure 6, the number of the O···O bonds per oxygen atom in the DMA−water mixtures is plotted as a function of x_{DMA}, together with that for pure water, which was determined in the previous study (3.43 ± 0.12).[4] The number of O···O bonds increases monotonically as the water content increases in the x_{DMA} range of 0.7−0.9, but then increases sharply at $x_{DMA} = 0.6$, again monotonically at $x_{DMA} = 0.5$−0.1, and insignificantly at $x_{DMA} < 0.1$. Thus, there are two inflection points in the number of hydrogen bonds, at $x_{DMA} = 0.1$ and 0.6. The inflection points are in good agreement with those observed in the wavenumber of the ν_{O-D} mode. This coincidence strongly suggests that the hydrogen bonds among water molecules grow up to form the tetrahedral-like structure of water in the DMA−water mixtures at $x_{DMA} = 0.6$, and the water structure is predominantly evolved in the mixtures at $x_{DMA} = 0.1$.

On the basis of the present results from both IR and XRD experiments, the structure of the DMA−water mixtures can be classified into four regimes: (1) at $x_{DMA} = 0.60$−1, the inherent structure of DMA is dominant; (2) at $x_{DMA} = 0.40$−0.60, both DMA and water structures coexist, but the former is gradually disrupted, whereas the latter increases; (3) at $0.10 < x_{DMA} \leq 0.30$, more water structure than the DMA structure is formed; and finally, (4) at $x_{DMA} \leq 0.10$, the tetrahedral-like water network predominates in the mixture. It is probable that DMA molecules are embedded in the water network.

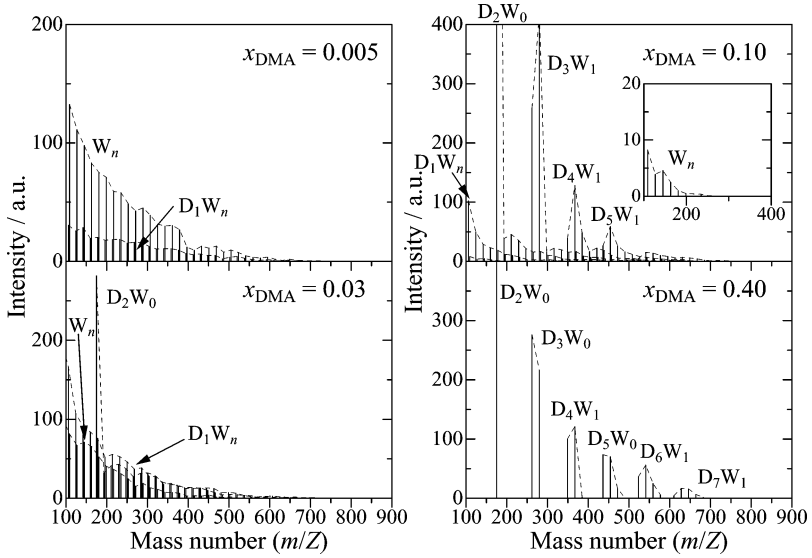

Figure 7. Mass spectra of the clusters isolated from liquid droplets of DMA−water mixtures at x_{DMA} = 0.005, 0.03, 0.10, and 0.40. The intensity-enhanced spectrum in the mass-number range of 100 ≤ m/Z ≤ 400 is superimposed in the mass spectrum at x_{DMA} = 0.10.

Mass Spectrometry. Figure 7 shows the mass spectra of the clusters over the mass-number range of 100 ≤ m/Z ≤ 900, isolated from liquid droplets of the DMA−water mixtures at x_{DMA} = 0.005, 0.03, 0.10, and 0.40. In the ionization process with an electron impact energy of 40 eV, an OH radical is eliminated from a water molecule within a cluster. Therefore, the mass signals of DMA−water and water clusters, abbreviated as $H^+D_mW_n$ and H^+W_n, respectively, are observed in the mass spectra; D and W represent DMA and water molecules, respectively, and m and n give the number of the respective molecules in the clusters. One must also note that some of the water molecules are evaporated upon electron impact ionization of the original clusters. Hereafter, clusters of $H^+D_mW_n$ and H^+W_n are shortened to D_mW_n and W_n, respectively.

As seen in Figure 7, the mass spectral pattern drastically changes with x_{DMA}. In the mass spectrum at x_{DMA} = 0.005, the signal sequence of water clusters (W_n) is observed dominantly, in addition to that of the D_1W_n clusters. In the present experiments, signal sequences of the D_2W_n and D_3W_n clusters are also detected; however, their signals cannot be seen in the figure, because of the very weak intensities. The spectrum at x_{DMA} = 0.03 shows that the W_n and D_1W_n clusters are both dominant. These findings are consistent with the present results from IR spectroscopy and XRD, i.e., the tetrahedral-like structure of water predominates in the mixture at x_{DMA} ≤ 0.10 and DMA molecules are probably embedded in the water network. The signal sequence of D_2W_n clusters appears in the range of 175 ≤ m/Z ≤ 751, where the strongest signal is assigned to the nonhydrated dimer D_2W_0, as indicated in the spectrum.

At x_{DMA} = 0.10, the signals of the W_n and D_1W_n clusters become weak, whereas those for the oligomer DMA clusters, such as D_3W_n, D_4W_n, and D_5W_n, are significant, as well as that of the D_2W_n cluster. The strongest intensities in the signal sequences are represented in the figure, e.g., D_3W_1 and D_4W_1. When the value of x_{DMA} is increased to 0.40, the signal sequences of the W_n and D_1W_n clusters completely disappear, and those of the oligomer DMA clusters up to D_8W_n (whose signals, however, cannot be seen in the figure, because of the weak intensities) are detected in the present mass-number range. The strongest intensities in the signal sequences of the oligomer DMA clusters are assigned to nonhydrated D_mW_0 or monohydrated D_mW_1 clusters. The observation of the mass signals for the large oligomers, such as D_8W_n, suggests that intermolecular interactions among DMA molecules are strengthened in the mixtures by a hydrophobic effect. Under the present conditions, however, the mass signals of DMA aggregates were not detected at x_{DMA} > 0.4, whereas signal intensities of oligomer alcohol clusters were observed for methanol−water[4] and ethanol−water[5−7] mixtures over the alcohol mole fraction range of 0.1−0.9. This is because the predominant DMA clusters formed by the weak dipole−dipole and hydrophobic interactions among them, but not strong hydrogen bonds, in the liquid droplets are easily disrupted through the adiabatic expansion process.

To estimate the number of water molecules within the W_n cluster and the average hydration number for the D_1W_n−D_8W_n clusters, the mass-signal sequences of the clusters were fitted by Γ and Gaussian distributions, and their combination using a least-squares procedure. As discussed in the previous investigations on methanol−water[4] and ethanol−water[6,7] mixtures, mass-signal sequences can often be reproduced well by empirical distribution functions, such as the Boltzmann and Poisson functions, and the functions give us the average hydration numbers of clusters observed. The details of the fitting procedure are described in the Supporting Information.

The Gaussian and Γ components of the mass-signal sequences can be assigned as follows. The Gaussian components observed in the signal sequences of the D_3W_n−D_8W_n clusters may arise from hydrogen-bonded DMA−water clusters, where water molecules bind to the carbonyl oxygen atoms of DMA molecules through hydrogen bonding. On the other hand, the Γ components more widely appear in the larger hydration number range than the Gaussian components but disappear at low water contents (x_{DMA} > 0.10). This implies that many water molecules weakly surround DMA clusters. Thus, the Γ component in the signal sequences of the D_2W_n−D_8W_n clusters may be attributed to the DMA clusters, which are surrounded by water molecules through weak interaction, such as dipole−dipole interaction between the DMA and water molecules.

Figure 8 shows the average hydration numbers $\langle n_m^G \rangle$ of the D_3W_n−D_8W_n clusters, as estimated from the Gaussian components, as a function of x_{DMA}. The x_{DMA} dependence of the average hydration number can be explained by a Γ distribution function. The Γ distribution functions obtained from a least-squares fitting procedure are listed in Table S3 in the Supporting

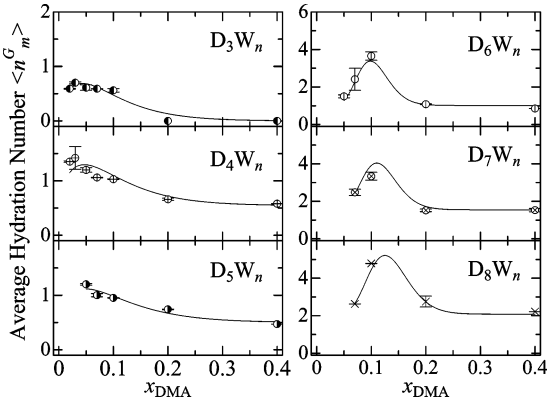

Figure 8. Plots of average hydration numbers $\langle n_m^G \rangle$ of the $D_3W_n-D_8W_n$ clusters estimated from the corresponding Gaussian components in the mass signal sequences, as a function of x_{DMA}. The standard deviations (σ) were depicted as error bars. Solid lines are Γ distribution functions calculated using the equations in Table S3 (in the Supporting Information).

Information and are depicted by the solid lines in Figure 8. As shown in this figure, the average hydration numbers of the oligomer DMA clusters of D_3W_n, D_4W_n, and D_5W_n exhibit a maximum at $x_{DMA} = 0.05$ with $\langle n_m^G \rangle = 0.5-1.0$ and decay toward 0 or 0.5 with increasing x_{DMA}. On the other hand, the average hydration numbers of the D_6W_n, D_7W_n, and D_8W_n clusters increase when the value of x_{DMA} increases and reach a maximum at $x_{DMA} = 0.10$. Then, the values decrease down to 1−2 with further increases in x_{DMA}. The maximum hydration numbers (4−5) of D_6W_n, D_7W_n, and D_8W_n clusters are larger than those for D_3W_n, D_4W_n, and D_5W_n clusters, suggesting that the larger the oligomer DMA clusters that are formed, the more the water molecules bind to DMA molecules, because of the increase in the hydrogen bonding sites within the clusters.

Figure 9 shows the x_{DMA} dependence of the average number of water molecules within the W_n clusters and the average hydration numbers of the $D_1W_n-D_6W_n$ clusters, which are estimated from the Γ components, respectively. The $\langle n_m^\Gamma \rangle$ values were fitted by a least-squares fitting procedure with a Γ distribution function. Table S3 in the Supporting Information shows a summary of the Γ distribution functions that have been refined, and the optimized values are represented by the solid lines in Figure 9. The average number of water molecules within the W_n clusters increases as the value of x_{DMA} increases and exhibits a maximum at $x_{DMA} = 0.01$ with $\langle n_m^\Gamma \rangle = 10$. With further increasing of the value of x_{DMA} up to 0.10, the $\langle n_m^\Gamma \rangle$ value gradually decreases down to 3. The changes in the average hydration numbers of the D_1W_n and D_2W_n clusters, relative to x_{DMA}, are similar to that of the W_n clusters. However, the maximum hydration number of D_1W_n clusters (23) is larger than the number of water molecules within the W_n clusters (10). It is suggested that the tetrahedral-like structure of water is more stabilized around a DMA molecule than that in pure water, because of hydration of the DMA molecule; i.e., the DMA molecule is embedded in the water network, as discussed in the IR and XRD sections. However, the maximum hydration number (9) of the D_2W_n clusters is comparable with that of the W_n clusters. When the number m for the D_mW_n cluster increases from 3 to 6, the maximum hydration number is suppressed from 9 to 3.

These results from the present mass spectrometric experiments show the specific mole fraction of $x_{DMA} = 0.10$. The specific mole fraction may be related to the tetrahedral-like structure of water formed in the bulk mixtures. In fact, the present results from the IR and XRD experiments on the bulk mixtures show that the water network is dominant in the DMA−water mixtures with $x_{DMA} < 0.10$, whereas DMA clusters gradually increase in the mixtures with $x_{DMA} > 0.10$.

Structure of DMA−Water Mixtures. On the basis of all the present results, possible structural changes in the DMA−water mixtures, relative to x_{DMA}, are clarified as follows. In the water-rich range of $0 < x_{DMA} \leq 0.1$, the tetrahedral-like structure of water predominates in the mixtures; the RDFs of the DMA−water mixtures at $x_{DMA} \leq 0.1$ bear good resemblance to that of pure water. The wavenumbers of the ν_{O-D} band of HDO in the mixtures and the numbers of hydrogen bonds estimated from the RDFs are almost constant at those for pure water, respectively. Furthermore, the mass signals of W_n clusters isolated from the bulk DMA−water mixtures are observed in the mass spectra at $x_{DMA} \leq 0.1$ but not $x_{DMA} > 0.1$. In the lower x_{DMA} range, DMA molecules may be surrounded by many water molecules in the water network.

In the range of $0.1 < x_{DMA} \leq 0.3$, the tetrahedral-like structure of water gradually decreases as the DMA content increases, whereas the number of DMA clusters increases in the mixtures, under the same conditions. However, more water clusters are formed than DMA clusters, because the second- and third-neighbor interactions of water molecules in the water network are still observed in the RDFs of the mixtures in this x_{DMA} range. When the DMA mole fraction further increases up to $x_{DMA} = 0.4$, the RDF is comparable to that of pure DMA, rather than that of pure water; the broad hump at 3.8−8 Å is characteristic of the intermolecular interactions among DMA molecules. In addition, the signal sequences of the various oligomer DMA

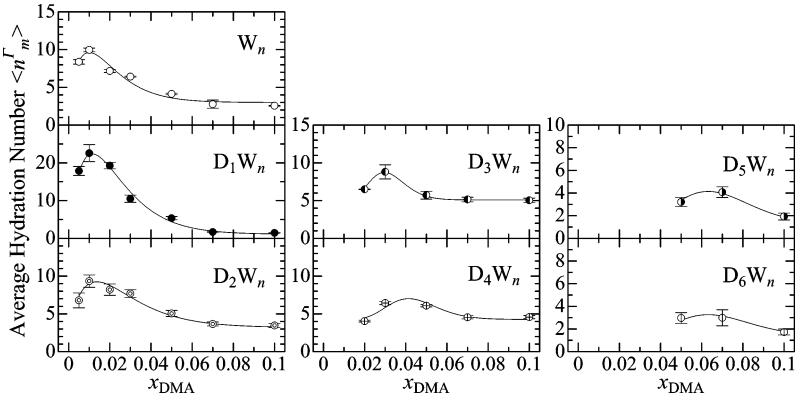

Figure 9. Plots of average hydration numbers $\langle n_m^\Gamma \rangle$ of the $D_1W_n-D_6W_n$ clusters estimated from the corresponding Γ components in the mass signal sequences as a function of x_{DMA}. The standard deviations (σ) were depicted as error bars. Solid lines are Γ distribution functions calculated using the equations in Table S3 (in the Supporting Information).

clusters are dominant in the mass spectra at $x_{DMA} = 0.4$. It is suggested that DMA clusters significantly increase in the DMA−water mixtures. However, the ν_{O-D} band of HDO in the mixtures reveals that the tetrahedral-like structure of water still remains in the mixtures.

The sudden increase in the wavenumber of the ν_{O-D} band of HDO in the mixtures at $x_{DMA} \approx 0.6$ implies that the tetrahedral-like structure of water is disrupted in the mixtures. It is thus concluded that the inherent structure of DMA observed in pure DMA is dominant in the DMA−water mixtures in the range of $0.6 \leq x_{DMA} < 1$.

Here, the structures of the aqueous mixtures of organic solvents (DMA−water, 1,4-dioxane−water,[8] and acetonitrile−water[9−11]) are compared to each other at the molecular level. The tetrahedral-like structure of water predominates in the mixtures at organic solvent mole fractions of $x \leq 0.1$. However, those of the mixtures at $x \geq 0.1$ are dependent on the characteristics of the organic solvent molecules. In 1,4-dioxane−water mixtures,[8] small binary clusters of one or two 1,4-dioxane molecules and several water molecules hydrogen-bonded to them are formed at $0.15 \leq x \leq 0.2$. At $x \geq 0.3$, the inherent structure of 1,4-dioxane is dominant, and water molecules are involved in the 1,4-dioxane structure by hydrogen bonding. Thus, 1,4-dioxane−water hydrogen bonds mainly govern the structure of 1,4-dioxane−water mixtures. In acetonitrile−water mixtures,[9−11] in the wide range of $0.2 \leq x \leq 0.6$, both water clusters and acetonitrile clusters coexist in acetonitrile−water mixtures. However, both clusters weakly interact with the dipole−dipole interaction between the acetonitrile and water molecules but not the strong hydrogen bonds between them. Hence, microheterogeneity occurs in acetonitrile−water mixtures. The present investigation shows that DMA molecules aggregate with the dipole−dipole interactions among DMA molecules to form DMA clusters as well as acetonitrile molecules. In contrast with the acetonitrile molecule, however, the C═O···HOH hydrogen bond between the DMA and water molecules is strong in DMA−water mixtures, as is the case for 1,4-dioxane molecules. It is thus concluded that both characteristics of the DMA molecule lead to the intermediate mixing state of DMA−water mixtures between the 1,4-dioxane−water and acetonitrile−water mixtures; i.e., DMA clusters and water clusters both are formed in the mixtures as well as in the acetonitrile−water mixtures. At the same time, DMA clusters and water clusters are partially bridged with the C═O···HOH hydrogen bonds between DMA and water molecules, resulting in a mixing of the DMA and water molecules at any mixing ratio.

The enthalpies of mixing for DMA−water mixtures at 298 K are negative over the entire range of x_{DMA} values, with a minimum of -3600 J mol^{-1} at $x_{DMA} = 0.33$,[32] which is surprisingly fairly negative, in comparison with those for methanol−water and ethanol−water mixtures (-850 J mol^{-1} at a methanol mole fraction of $x_M = 0.3$ and -730 J mol^{-1} at an ethanol mole fraction of $x_E = 0.2$, respectively[33]). The greatly negative enthalpies of mixing for DMA−water mixtures may arise from stabilization of the DMA−DMA interaction, i.e., DMA−DMA interaction will be stabilized by the C═O···HOH hydrogen bonds and hydrophobic effect upon the addition of water, whereas DMA molecules weakly interact each other in the liquid. On the other hand, methanol and ethanol molecules are originally stable in the liquids, because of hydrogen bonding among them, resulting in an insignificant gain by the addition of water.

The present results also show that the DMA−water mixtures have an intermediate structure between that of pure DMA and that of pure water in the range of $0.3 \leq x_{DMA} \leq 0.4$; DMA and water clusters coexist in the DMA−water mixtures. It is very likely that the DMA−DMA interaction is most strengthened at this mole fraction range by a bridge between the DMA and the water clusters with C═O···HOH hydrogen bonding and a hydrophobic effect, because this is the most stable mixing state of DMA−water mixtures at $x_{DMA} = 0.33$. On the other hand, the disruption of the tetrahedral-like structure of water or DMA clusters will cause an enthalpic loss at other x_{DMA} values. Thus, the minimum of the enthalpies of mixing[32] and the largest deviations of the various properties from ideality are observed at $x_{DMA} = 0.33$.[1]

Acknowledgment. This work was supported partly by the Joint Studies Program (1998−2001) of the Institute for Molecular Science and by Grants-in-Aid (Nos. 09740444 and 12640500) (T.T.) from the Ministry of Education, Culture, Sports, Science, and Technology, Japan.

Supporting Information Available: Structure functions for DMA, water, and DMA−water mixtures (Figure S1), signal sequences of D_1W_n, D_2W_n, D_4W_n, and D_7W_n clusters (Figures S2−S5), intramolecular interactions for DMA and water molecules (Table S1), optimized structural parameters in DMA−water mixtures (Table S2), optimized Γ distribution function (Table S3), and details of the fitting procedure on the mass signal sequences. This material is available free of charge via the Internet at http://pubs.acs.org.

References and Notes

(1) Kinart, C. M.; Kinart, W. J.; Bald, A.; Szejgis, A. *Phys. Chem. Liq.* **1995**, *30*, 151.
(2) Józwiak, M.; Piekarski, H. *J. Mol. Liq.* **1999**, *81*, 63.
(3) Józwiak, M. *J. Mol. Liq.* **1999**, *81*, 261.
(4) Takamuku, T.; Yamaguchi, T.; Asato, M.; Matsumoto, M.; Nishi, N. *Z. Naturforsch., A: Phys. Sci.* **2000**, *55*, 513.
(5) Nishi, N.; Takahashi, S.; Matsumoto, M.; Tanaka, A.; Muraya, K.; Takamuku, T.; Yamaguchi, T. *J. Phys. Chem.* **1995**, *99*, 462.
(6) Matsumoto, M.; Nishi, N.; Furusawa, T.; Saita, M.; Takamuku, T.; Yamagami, M.; Yamaguchi, T. *Bull. Chem. Soc. Jpn.* **1995**, *68*, 1775.
(7) Nishi, N.; Matsumoto, M.; Takahashi, S.; Takamuku, T.; Yamagami, M.; Yamaguchi, T. *Structures and Dynamics of Clusters*; Kondow, T., Kaya, K., Terasaki, A., Eds.; Universal Academy Press, Inc., Yamada Science Foundation: Tokyo, 1996; pp 113−120.
(8) Takamuku, T.; Yamaguchi, A.; Tabata, M.; Nishi, N.; Yoshida, K.; Wakita, H.; Yamaguchi, T. *J. Mol. Liq.* **1999**, *83*, 163.
(9) Takamuku, T.; Tabata, M.; Yamaguchi, A.; Nishimoto, J.; Kumamoto, M.; Wakita, H.; Yamaguchi, T. *J. Phys. Chem. B* **1998**, *102*, 8880.
(10) Takamuku, T.; Matsuo, D.; Yamaguchi, A.; Tabata, M.; Yoshida, K.; Yamaguchi, T.; Nagao, M.; Otomo, T.; Adachi, T. *Chem. Lett.* **2000**, 878.
(11) Takamuku, T.; Yamaguchi, A.; Matsuo, D.; Tabata, M.; Kumamoto, M.; Nishimoto, J.; Yoshida, K.; Yamaguchi, T.; Nagao, M.; Otomo, T.; Adachi, T. *J. Phys. Chem. B* **2001**, *105*, 6236.
(12) Yamanaka, K.; Yamaguchi, T.; Wakita, H. *J. Chem. Phys.* **1994**, *101*, 9830.
(13) Ihara, M.; Yamaguchi, T.; Wakita, H.; Matsumoto, T. *Adv. X-ray Anal. Jpn.* **1994**, *25*, 49. Yamaguchi, T.; Wakita, H.; Yamanaka, K. *Fukuoka Daigaku Rigaku Shuho* **1999**, *29*, 127.
(14) Furukawa, K. *Rep. Progr. Phys.* **1962**, *25*, 395.
(15) Krogh-Moe, J. *Acta Crystallogr.* **1956**, *2*, 951.
(16) Norman, N. *Acta Crystallogr.* **1957**, *10*, 370.
(17) Johanson, G.; Sandström, M. *Chem. Scr.* **1973**, *4*, 195.
(18) Yamaguchi, T. Doctoral Thesis, Tokyo Institute of Technology, Tokyo, 1978.
(19) Nishi, N.; Koga, K.; Ohshima, C.; Yamamoto, K.; Nagashima, U.; Nagami, K. *J. Am. Chem. Soc.* **1988**, *110*, 5246.
(20) Nishi, N. *Z. Phys. D: At., Mol. Clusters* **1990**, *15*, 239.
(21) Nishi, N.; Yamamoto, K. *J. Am. Chem. Soc.* **1987**, *109*, 7353.

(22) Yamamoto, K.; Nishi, N. *J. Am. Chem. Soc.* **1990**, *112*, 549.
(23) Yamamoto, O.; Someno, K.; Wasada, N.; Hiraishi, J.; Hayamizu, K.; Tanabe, K.; Yanagisawa, M. *Anal. Sci.* **1988**, *4*, 233.
(24) Mizuno, K.; Ochi, T.; Shindo, Y. *J. Chem. Phys.* **1998**, *109*, 9502.
(25) Furutaka, S.; Ikawa, S. *J. Chem. Phys.* **1998**, *108*, 1347.
(26) Mack, H.-G.; Oberhammer, H. *J. Am. Chem. Soc.* **1997**, *119*, 3567.
(27) Ohtaki, H.; Itoh, S.; Yamaguchi, T.; Ishiguro, S.; Rode, B. M. *Bull. Chem. Soc. Jpn.* **1983**, *56*, 3406.
(28) Ichikawa, K.; Kameda, Y.; Yamaguchi, T.; Wakita, H.; Misawa, M. *Mol. Phys.* **1991**, *73*, 79.
(29) Narten, A. H.; Levy, H. A. *J. Chem. Phys.* **1971**, *55*, 2263.
(30) Narten, A. H. *J. Chem. Phys.* **1972**, *56*, 5681.
(31) Gutmann, V. *The Donor−Acceptor Approach to Molecular Interactions*; Plenum Press: New York, 1978.
(32) Stokes, R. H. *J. Chem. Thermodyn.* **1987**, *19*, 1155.
(33) Franks, F.; Ives, D. J. G. *Q. Rev. Chem. Soc.* **1966**, *20*, 1.